Journal of Zhejiang University-SCIENCE B 2026 27(4):359-374
www.jzus.zju.edu.cn; www.springer.com/journal/11585
E-mail: jzus_b@zju.edu.cn

Research Article
https://doi.org/10.1631/jzus.B2500567

Check for updates

TAF1 aggravates ferroptosis by promoting the ubiquitin-mediated degradation of nuclear GPX4

Kehong YE[1,2], Meifu GAN[3], Liang SUN[1], Chaoyi CHEN[4], Xuan LAI[1], Yinjun HE[5], Ming ZHU[1], Weiqin JIANG[6]✉, Honghe ZHANG[1]✉

[1]*Department of Pathology, Zhejiang University School of Medicine, Hangzhou 310058, China*
[2]*Department of Pathology, Zhejiang Cancer Hospital, Hangzhou Institute of Medicine (HIM), Chinese Academy of Sciences, Hangzhou 310022, China*
[3]*Taizhou Hospital of Zhejiang Province Affiliated to Wenzhou Medical University, Taizhou 317000, China*
[4]*Department of Colorectal Surgery and Oncology (Key Laboratory of Cancer Prevention and Intervention, China National Ministry of Education, Key Laboratory of Molecular Biology in Medical Sciences, Zhejiang Province, China), The Second Affiliated Hospital, Zhejiang University School of Medicine, Hangzhou 310009, China*
[5]*Department of Pathology, State Key Laboratory of Complex Severe and Rare Disease, Molecular Pathology Research Center, Peking Union Medical College Hospital, Chinese Academy of Medical Sciences and Peking Union Medical College, Beijing 100730, China*
[6]*Department of Colorectal Surgery and Oncology, The First Affiliated Hospital, Zhejiang University School of Medicine, Hangzhou 310006, China*

Abstract: Glutathione peroxidase 4 (GPX4) is a primary inhibitor of ferroptosis, a regulated form of cell death driven by the accumulation of lipid hydroperoxides. GPX4 exists in three isoforms localized in the cytosol, mitochondria, and nucleus; however, the regulatory mechanisms governing nuclear GPX4 (nGPX4) remain largely unclear. Herein, we identified TATA box-binding protein-associated factor 1 (TAF1) as a pivotal regulator of nGPX4. TAF1 phosphorylates nGPX4, leading to its lysine 11 (K11)-linked ubiquitination and proteasomal degradation, thereby promoting ferroptosis in tumor protein p53 (*TP53*)-mutant cells. Conversely, in *TP53*-wild-type (WT) cells, TAF1 phosphorylates TP53, facilitating murine double minute 2 (MDM2)-mediated TP53 degradation, which upregulates solute carrier family 7 member 11 (*SLC7A11*) expression and reduces cellular susceptibility to ferroptosis. Collectively, TAF1 plays dual and context-dependent roles in ferroptosis regulation, acting as both a promoter and an inhibitor depending on the *TP53* status.

Key words: TATA box-binding protein-associated factor 1 (TAF1); Tumor protein p53 (TP53); Ferroptosis; Glutathione peroxidase 4 (GPX4); Protein degradation

1 Introduction

TATA box-binding protein-associated factor 1 (TAF1), the largest subunit of the general transcription factor TFIID (Wang et al., 2014), is a key component of the RNA polymerase II transcription machinery and has been implicated in several neurodegenerative disorders, including X-linked dystonia-parkinsonism (XDP) (Aneichyk et al., 2018), X-linked syndromic mental retardation-33 (MRXS33) (Cheng et al., 2020), and TAF1 intellectual disability syndrome (TAF1 ID syndrome) (Janakiraman et al., 2020). Beyond its role in neurodegeneration, TAF1 also participates in tumorigenesis and cancer progression. Elevated *TAF1* expression has been reported in various tumor types (Zhou et al., 2021), and *TAF1* mutations have been associated with gastric, colorectal, and ovarian cancers (Ribeiro et al., 2014; Oh et al., 2017). Notably, such mutations occur more frequently in peritoneal carcinomatosis than in primary gastric adenocarcinoma (Wang et al., 2020), suggesting the potential role of *TAF1* in promoting metastatic dissemination. Structurally, TAF1 comprises an N-terminal kinase domain, a C-terminal kinase domain (Dikstein et al., 1996), a histone acetyltransferase

✉ Honghe ZHANG, honghezhang@zju.edu.cn
Weiqin JIANG, weiqinjiang@zju.edu.cn
Honghe ZHANG, https://orcid.org/0000-0001-5954-2857
Weiqin JIANG, https://orcid.org/0000-0003-3200-8835
Kehong YE, https://orcid.org/0000-0002-3364-7850

Received Sept. 8, 2025; Revision accepted Nov. 11, 2025; Crosschecked Apr. 17, 2026

(HAT) domain (Mizzen et al., 1996), and an E1/E2 ubiquitin-activating/conjugating domain (Pham and Sauer, 2000), each conferring distinct regulatory functions in cancer biology (Tavassoli et al., 2010; Xu et al., 2019).

Ferroptosis, a recently discovered form of regulated cell death, is driven by the accumulation of iron-dependent phospholipid hydroperoxides (Dixon et al., 2012). These are generated either through lipoxygenase activity or by reactive oxygen species (ROS) derived from membrane electron transport proteins attacking polyunsaturated fatty acids (PUFAs) (Chen et al., 2021). The detoxification of phospholipid hydroperoxides depends on several antioxidant systems, including the solute carrier family 7 member 11 (SLC7A11)–glutathione (GSH)–glutathione peroxidase 4 (GPX4) pathway (Dixon et al., 2014; Yang et al., 2014), the coenzyme Q10 (CoQ10)–ferroptosis suppressor protein 1 (FSP1) pathway (Doll et al., 2019), and the CoQ10–dihydroorotate dehydrogenase (DHODH) pathway (Mao et al., 2021). Among these, the most extensively studied pathway is SLC7A11–GSH–GPX4. At the core of this pathway is GPX4, a selenoprotein (Yang et al., 2016; Xie et al., 2023) that utilizes GSH to reduce lipid peroxides to their corresponding alcohols (Yang et al., 2014). GPX4 exists in three isoforms—cytoplasmic (cGPX4), mitochondrial (mGPX4), and nuclear (nGPX4). While the functions and regulatory mechanisms of cGPX4 and mGPX4 have been well characterized (Deng et al., 2021; Qian et al., 2023; Guo et al., 2024; Xie et al., 2024), those of nGPX4 remain poorly understood.

In this study, we identified TAF1 as a critical regulator of ferroptosis whose function depends on the tumor protein p53 (*TP53*) status. In *TP53*-wild-type (WT) cells, TAF1 alleviates ferroptosis by promoting TP53 degradation, thereby upregulating *SLC7A11* expression. In contrast, in *TP53*-mutant cells, TAF1 promotes ferroptosis by facilitating the lysine 11 (K11)-linked ubiquitination and proteasomal degradation of nGPX4. These findings uncover a previously unrecognized mechanism linking TAF1 to ferroptosis regulation.

2 Results

2.1 TAF1 as a potential driver of ferroptosis

In order to identify potential ferroptosis drivers, we analyzed the National Cancer Institute Genomic Data Commons (GDC) Pan-Cancer dataset using the University of California, Santa Cruz (UCSC) Xena Browser (https://xenabrowser.net) (Goldman et al., 2020). This analysis revealed that the messenger RNA (mRNA) expression levels of 177 genes were negatively correlated with those of four canonical ferroptosis suppressors, including *GPX4*, *FSP1* (Bersuker et al., 2019), ferritin light chain (*FTL*), and ferritin heavy chain 1 (*FTH1*) (Hou et al., 2016) (Fig. 1a). Several of these genes have been previously implicated in apoptosis or necroptosis, such as never in mitosis gene A-related kinase 1 (*NEK1*) (Spies et al., 2016; Wang et al., 2021), α-thalassemia/mental retardation X-linked (ATRX) chromatin remodeler (*ATRX*) (Wang et al., 2024), and YT521-B homology (YTH) N^6-methyladenosine RNA-binding protein C1 (*YTHDC1*) (Feng et al., 2024).

In order to identify genes that may specifically regulate ferroptosis, we utilized a pro-apoptotic gene set, including B-cell lymphoma 2 (BCL2)-associated X (*BAX*), BCL2 antagonist/killer 1 (*BAK1*), cytochrome *c*, somatic (*CYCS*), apoptotic peptidase-activating factor 1 (*APAF1*), caspase 3 (*CASP3*), and *CASP7*, and a pro-necroptotic gene set, including receptor interacting serine/threonine kinase 1 (*RIPK1*), *RIPK3*, and mixed lineage kinase domain-like pseudokinase (*MLKL*) (Newton et al., 2024), to calculate pro-apoptosis and pro-necroptosis scores for each sample in the GDC Pan-Cancer dataset via gene set variation analysis (GSVA). Next, to identify those showing no association with apoptosis or necroptosis, we assessed the correlation between each score and the expression levels of the 177 genes (Fig. 1b). Considering that a Spearman's correlation coefficient $|\rho|<0.2$ indicates a poor or negligible correlation (Akoglu, 2018; Schober et al., 2018), we identified 90 genes exhibiting no significant association with either necroptosis or apoptosis (Fig. 1c).

Among these 90 genes, we further screened 27 genes whose expression levels were upregulated in colon adenocarcinoma (COAD) using Gene Expression Profiling Interactive Analysis 3 (GEPIA3) (https://gepia3.bioinfoliu.com) (Kang et al., 2025). Of these, three genes, namely pinin (*PNN*) (Lin et al., 2025), sacsin molecular chaperone (*SACS*) (Sun BH et al., 2023), and Ras-related nuclear protein (RAN)-binding protein 2 (*RANBP2*) (Zang et al., 2024) have been reported to regulate ferroptosis. The expression of the remaining 24 genes was subsequently examined in ovarian carcinoma

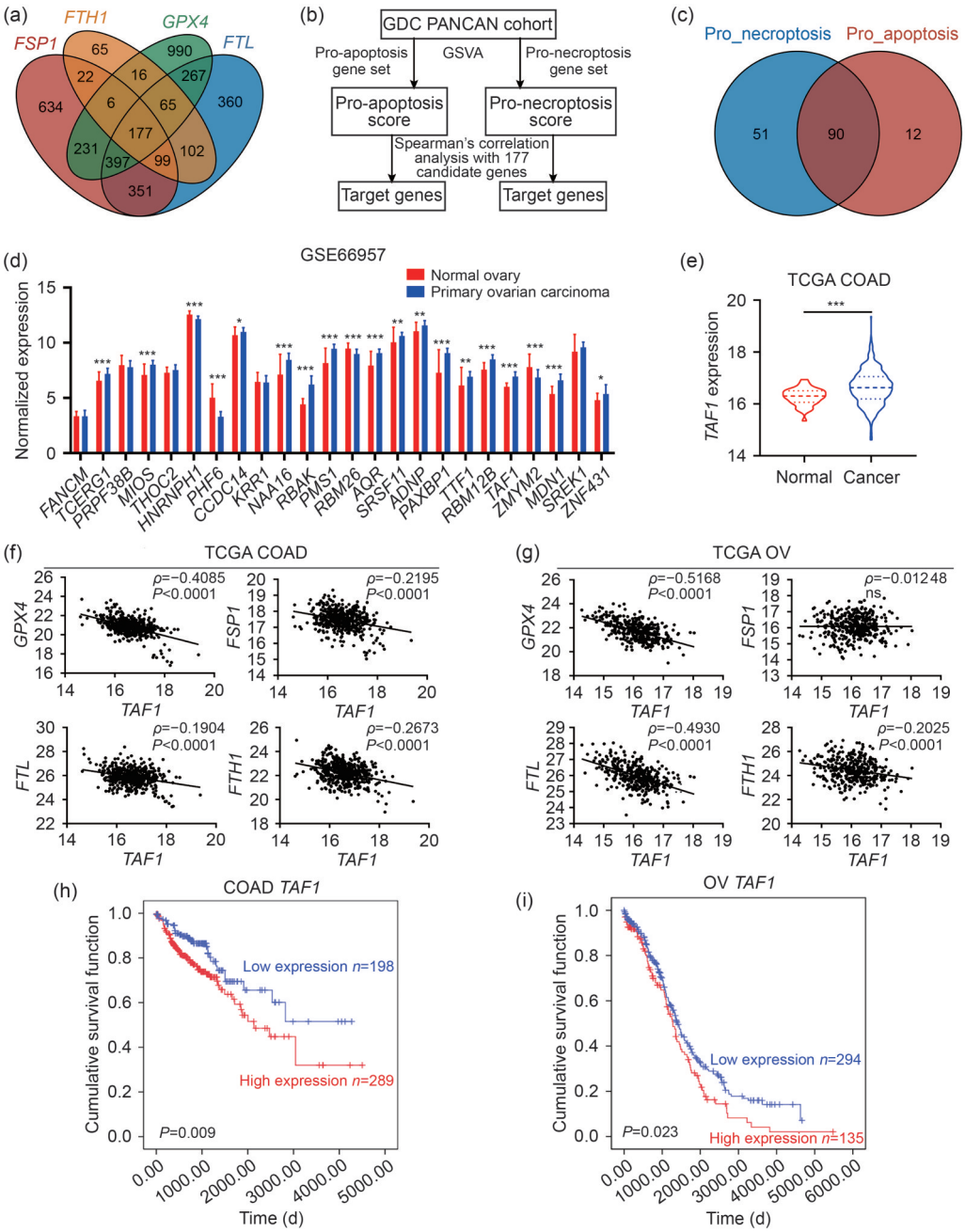

Fig. 1 TATA box-binding protein-associated factor 1 (TAF1) as a potential driver of ferroptosis. (a) Venn diagram showing the numbers of genes whose messenger RNA (mRNA) expression levels were negatively correlated with those of glutathione peroxidase 4 (*GPX4*), ferroptosis suppressor protein 1 (*FSP1*), ferritin heavy chain 1 (*FTH1*), and ferritin light chain (*FTL*) ($P<0.000\ 01$, $\rho<-0.23$). (b) Schematic representation of the screening strategy used to identify genes associated with apoptosis and necroptosis. (c) Venn diagram showing the numbers of genes that were not correlated with apoptosis or necroptosis ($|\rho|<0.2$). (d) Analysis of the mRNA expression levels of 24 candidate genes in ovarian serous cystadenocarcinoma tissues ($n=57$) and normal ovarian tissues ($n=12$) from the GSE66957 dataset. The data are expressed as mean±standard deviation (SD). (e) Analysis of *TAF1* mRNA levels in colon adenocarcinoma (COAD) tissues ($n=456$) and normal colon tissues ($n=41$) from The Cancer Genome Atlas (TCGA) database. Data are presented as median with interquartile range (IQR). (f, g) Dot plots depicting the correlations between the expression of *TAF1* and that of *GPX4*, *FSP1*, *FTH1*, and *FTL* in the TCGA COAD (f) and TCGA ovarian cancer (OV) (g) datasets. (h, i) Kaplan-Meier survival analyses of patients in the TCGA COAD (h) and TCGA OV (i) datasets. (a, c) Venn diagrams were generated using R software (v.4.2.2) package "VennDiagram" (v.1.7.3) through Hiplot^{Pro} (https://hiplot.com.cn), a comprehensive web service for biomedical data analysis and visualization. (d, e) $^{*}P<0.05$; $^{**}P<0.01$; $^{***}P<0.001$; two independent-sample Student's *t*-tests. GDC PANCAN: Genomic Data Commons Pan-Cancer; GSVA: gene set variation analysis.

patients using the GSE66957 dataset and we identified 14 genes upregulated in primary ovarian carcinoma (Fig. 1d). Among these, *TAF1* was consistently upregulated in both COAD and ovarian cancer (OV) (Fig. 1e) and was thus selected for further investigation.

We next examined the relationships between *TAF1* and ferroptosis suppressors in The Cancer Genome Atlas (TCGA) COAD and OV datasets. In COAD, *TAF1* mRNA expression was significantly and negatively correlated with all four canonical ferroptosis suppressors (*GPX4*, *FSP1*, *FTL*, and *FTH1*) (Fig. 1f). In OV, *TAF1* was negatively correlated with *GPX4*, *FTL*, and *FTH1*, but not with *FSP1* (Fig. 1g). Notably, the strongest inverse correlation across both cancer types consistently occurred between *TAF1* and *GPX4*, suggesting that TAF1 may act as a negative regulator of GPX4. Moreover, high *TAF1* expression was associated with poor prognosis in both COAD (Fig. 1h) and OV (Fig. 1i). Collectively, these findings indicate that TAF1 may function as a potential driver of ferroptosis, particularly in COAD and OV.

2.2 Distinct regulatory roles of TAF1 in ferroptosis

In order to determine whether TAF1 regulates ferroptosis, we first examined its protein expression in normal, COAD, and OV cell lines by western blotting (WB). As shown in Fig. 2a, TAF1 protein levels were markedly elevated in RKO (colorectal cancer (CRC)), SW620 (CRC), SKOV3 (OV), and A2780 (OV) cells compared with the normal human colon epithelial cell line NCM460. Using clustered regularly interspaced short palindromic repeats (CRISPR)/CRISPR-associated protein 9 (Cas9) technology, we established TAF1-knockout (TAF1-KO) cell lines (Figs. 2b–2e). These cells were subsequently treated with the GPX4 inhibitor (1S,3R)-RAS-selective lethal 3 (RSL3) to assess their sensitivity to ferroptosis. Interestingly, the effects of TAF1 loss varied among the cell lines. In SKOV3 and SW620 cells, TAF1 deficiency slightly increased resistance to RSL3 (Figs. 2f and S1a), whereas in RKO and A2780 cells, TAF1 KO markedly enhanced susceptibility to RSL3-induced ferroptosis (Figs. 2g and S1b).

Since the abnormal accumulation of ROS is a hallmark of ferroptosis, we next evaluated the ROS levels in TAF1-KO and Mock control cells under various conditions. In SKOV3 and SW620 Mock cells, RSL3 treatment significantly increased the ROS levels, which were reversed by ferrostatin-1 (a ferroptosis inhibitor) but not by *N*-benzyloxycarbonyl-Val-Ala-Asp(OMe)-fluoromethyl ketone (Z-VAD-FMK; an apoptosis inhibitor), necrostatin-1 (a necroptosis inhibitor), or chloroquine (CQ; an autophagy inhibitor). However, RSL3 failed to induce ROS accumulation in SKOV3 TAF1-KO cells. In SW620 TAF1-KO cells, elevated ROS levels were not suppressed by ferrostatin-1 (Figs. 2h and S1c).

In contrast, in RKO and A2780 TAF1-KO cells, RSL3 treatment significantly increased ROS levels, which were abrogated by ferrostatin-1 but not by Z-VAD-FMK, necrostatin-1, or CQ. Notably, RSL3 did not induce ROS accumulation in RKO or A2780 Mock cells (Figs. 2i and S1d).

We further assessed the lipid peroxidation (LPO) levels in tumor cells. Boron-dipyrromethene (BODIPY) staining revealed that RSL3 treatment markedly increased LPO in SKOV3 and SW620 TAF1-Mock cells, an effect that was completely rescued by ferrostatin-1 (Figs. 2j, 2k, S1e, and S1f). In contrast, RSL3 induced LPO accumulation only in RKO and A2780 TAF1-KO cells (Figs. 2l, 2m, S1g, and S1h).

Collectively, these results demonstrate that TAF1 exerts opposing effects on ferroptosis regulation depending on the cellular context, acting as either a suppressor or promoter of ferroptotic signaling.

2.3 Contrasting effects of TAF1 on ferroptosis depending on *TP53* status

In order to elucidate how TAF1 exerts opposing effects on ferroptosis, we examined the expression of the SLC7A11–GPX4 axis, the ferritinophagy pathway, and other key ferroptosis regulators, including TP53, acyl-CoA synthetase long chain family member 4 (ACSL4), and FSP1, in TAF1-Mock and TAF1-KO cells. Notably, the protein levels of TP53 were markedly elevated in RKO and A2780 TAF1-KO cells (Figs. 3a and 3b), but remained unchanged in SW620 TAF1-KO cells (Fig. 3c). According to the data from the Cancer Dependency Map (DepMap), RKO and A2780 cells express WT TP53, whereas SW620 cells harbor TP53 mutations (P309S and R273H) and SKOV3 cells are *TP53*-null (Fig. 3d). Previous studies have demonstrated that TAF1 phosphorylates WT TP53, promoting murine double minute 2 (MDM2)-mediated TP53 degradation (Li et al., 2004; Yang et al., 2019). These findings suggest that the contrasting effects of TAF1 on ferroptosis may depend on the *TP53* status.

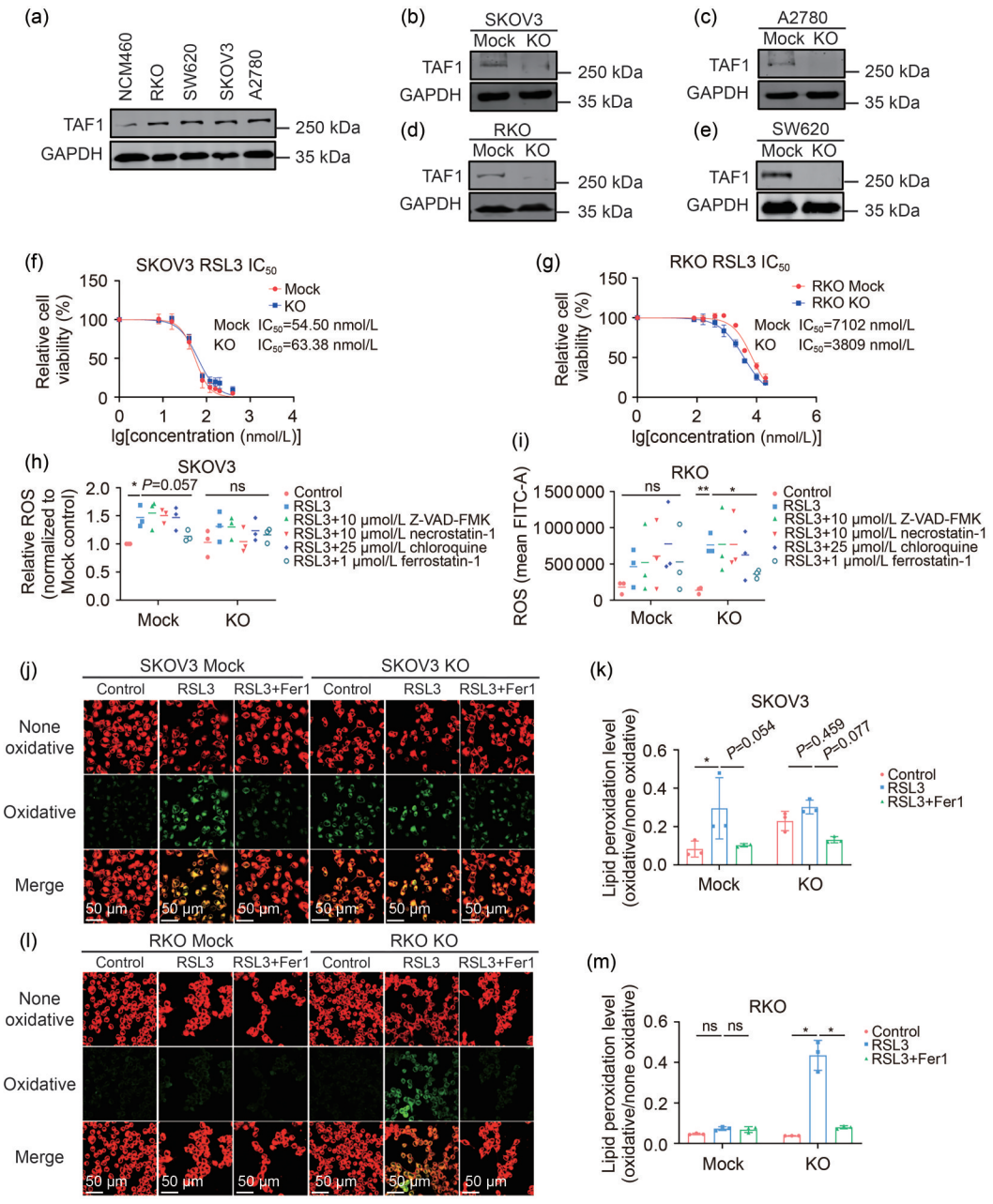

Fig. 2 Distinct regulatory roles of TATA box-binding protein-associated factor 1 (TAF1) in ferroptosis. (a) Western blotting (WB) analysis of TAF1 protein levels in NCM460, RKO, SW620, SKOV3, and A2780 cells. (b–e) Validation of TAF1 knockout (KO) in SKOV3 (b), A2780 (c), RKO (d), and SW620 (e) cells via WB. (f, g) Viability of TAF1-Mock and TAF1-KO cells treated with (1S,3R)-RAS-selective lethal 3 (RSL3) for 48 h at the indicated concentrations in SKOV3 (f) and RKO (g) cells. (h) Intracellular reactive oxygen species (ROS) levels in SKOV3 TAF1-Mock and TAF1-KO cells treated with 100 nmol/L RSL3 in the absence or presence of *N*-benzyloxycarbonyl-Val-Ala-Asp(OMe)-fluoromethyl ketone (Z-VAD-FMK), necrostatin-1, chloroquine (CQ), or ferrostatin-1 for 24 h. (i) Intracellular ROS levels in RKO TAF1-Mock and TAF1-KO cells treated with 6 μmol/L RSL3 in the absence or presence of Z-VAD-FMK, necrostatin-1, CQ, or ferrostatin-1 for 48 h. (j, k) Representative images (j) and quantitative analysis (k) of lipid peroxidation (LPO) in SKOV3 TAF1-Mock and TAF1-KO cells treated with 100 nmol/L RSL3 for 24 h with or without ferrostatin-1. (l, m) Representative images (l) and quantitative analysis (m) of LPO in RKO TAF1-Mock and TAF1-KO cells treated with 6 μmol/L RSL3 for 48 h with or without ferrostatin-1. All experiments were performed in triplicate. The data are presented as mean±standard deviation (SD) (f, g, k, m) or mean (h, i) (n=3). $^{*}P$<0.05; $^{**}P$<0.01; ns (not significant), P>0.05; paired Student's t-tests (h, i) and one-way analysis of variance (ANOVA) (k, m). GAPDH: glyceraldehyde-3-phosphate dehydrogenase; IC_{50}: half maximal inhibitory concentration; FITC-A: fluorescein isothiocyanate-area; Fer1: ferrostatin-1.

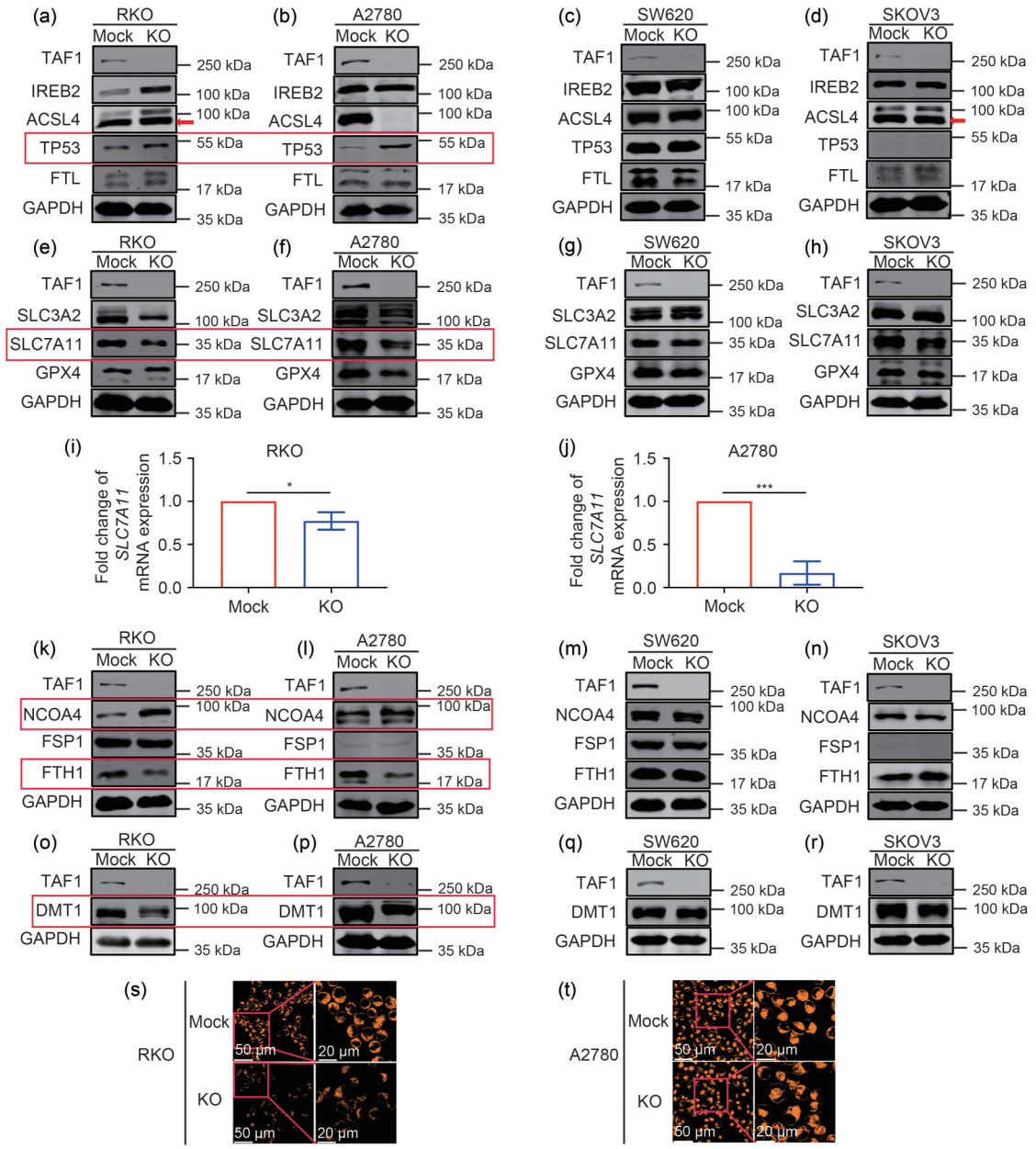

Fig. 3 Contrasting effects of TATA box-binding protein-associated factor 1 (TAF1) on ferroptosis depending on tumor protein p53 (*TP53*) status. (a–d) Western blotting (WB) analysis of iron-responsive element-binding protein 2 (IREB2), acyl-CoA synthetase long chain family member 4 (ACSL4), TP53, and ferritin light chain (FTL) protein levels in TAF1-Mock and TAF1-knockout (KO) cells of RKO (a), A2780 (b), SW620 (c), and SKOV3 (d). The red arrow indicates the expected position of the ACSL4 band. The red box highlights the protein with the most pronounced change. (e–h) WB analysis of the solute carrier family 3 member 2 (SLC3A2), solute carrier family 7 member 11 (SLC7A11), and glutathione peroxidase 4 (GPX4) protein levels in TAF1-Mock and TAF1-KO cells of RKO (e), A2780 (f), SW620 (g), and SKOV3 (h). The red box highlights the protein with the most pronounced change. (i, j) Relative messenger RNA (mRNA) expression levels of *SLC7A11* in TAF1-Mock and TAF1-KO cells of RKO (i) and A2780 (j). All experiments were performed in triplicate. The data are presented as mean±standard deviation (SD). $^{*}P<0.05$; $^{***}P<0.001$; two independent-sample Student's *t*-tests. (k–n) WB analysis of nuclear receptor coactivator 4 (NCOA4), ferroptosis suppressor protein 1 (FSP1), and ferritin heavy chain 1 (FTH1) protein levels in TAF1-Mock and TAF1-KO cells of RKO (k), A2780 (l), SW620 (m), and SKOV3 (n). The red box highlights the protein with the most pronounced change. (o–r) WB analysis of divalent metal transporter 1 (DMT1) protein levels in TAF1-Mock and TAF1-KO cells of RKO (o), A2780 (p), SW620 (q), and SKOV3 (r). The red box highlights the protein with the most pronounced change. (s, t) Cellular Fe^{2+} detection in TAF1-Mock and TAF1-KO cells of RKO (s) and A2780 (t) using immunofluorescence assays. GAPDH: glyceraldehyde-3-phosphate dehydrogenase.

We next analyzed SLC7A11, a canonical ferroptosis suppressor within the SLC7A11–GPX4 axis and a downstream target of TP53 (Jiang et al., 2015). The TAF1 KO in *TP53*-WT cells (RKO and A2780) significantly downregulated SLC7A11 protein expression (Figs. 3e and 3f), whereas no such change was observed in *TP53*-mutant or *TP53*-null cells (SW620 or SKOV3) (Figs. 3g and 3h). Consistent with the protein data, *SLC7A11* mRNA levels were also decreased in *TP53*-WT TAF1-KO cells, in agreement with previous reports (Jiang et al., 2015) (Figs. 3i and 3j).

In addition to SLC7A11, we found that TAF1 KO upregulated nuclear receptor coactivator 4 (NCOA4), a selective cargo receptor mediating ferritinophagy, thereby promoting ferritin degradation (Hou et al., 2016) in RKO and A2780 cells (Figs. 3k and 3l). However, no changes in NCOA4 expression were detected in *TP53*-mutant cells (Figs. 3m and 3n). Interestingly, TAF1 KO decreased the protein levels of FTH1 and divalent metal transporter 1 (DMT1) in both RKO and A2780 cells (Figs. 3k, 3l, 3o, and 3p), whereas no alteration was detected in SW620 or SKOV3 cells (Figs. 3m, 3n, 3q, and 3r), suggesting that TAF1 may also influence intracellular iron homeostasis in *TP53*-WT cells.

We next measured the levels of labile ferrous iron in TAF1-Mock and TAF1-KO cells. The deletion of TAF1 significantly reduced the labile iron pool in RKO cells (Fig. 3s) but did not alter the iron levels in A2780, SW620, or SKOV3 cells (Figs. 3t, S2a, and S2b). This discrepancy between labile iron levels and ferroptosis sensitivity in RKO and A2780 cells indicates that additional yet unidentified mechanisms may contribute to the cell-type-specific regulation of ferroptosis by TAF1.

Collectively, these findings demonstrate that TAF1 facilitates MDM2-mediated degradation of WT TP53, thereby upregulating *SLC7A11* expression and enhancing resistance to ferroptosis. These results highlight the pivotal role of *TP53* status in determining the dual regulatory effects of TAF1 on ferroptosis.

2.4 TAF1-mediated regulation of ferroptosis in *TP53*-mutant cells via ubiquitin-proteasome-mediated degradation of nGPX4

In order to further elucidate how TAF1 regulates ferroptosis in *TP53*-mutant cells, we explored its potential transcriptional and post-transcriptional roles. Given that TAF1 is the largest subunit of the TFIID complex, we initially hypothesized that TAF1 might influence ferroptosis through transcriptional regulation. To test this notion, we performed RNA sequencing (RNA-seq) analysis, which revealed no significant differences in the global transcriptome profiles following RSL3 or RSL3+ferrostatin-1 treatment in either SKOV3 TAF1-Mock or TAF1-KO cells (Fig. 4a). Differential expression and pathway enrichment analyses identified no ferroptosis-related genes or pathways in either the Gene Ontology (GO) or Kyoto Encyclopedia of Genes and Genomes (KEGG) database (Fig. S3).

Interestingly, TAF1 KO prevented the RSL3-induced reduction in GPX4 protein levels (Fig. 4b), while the *GPX4* mRNA levels remained unchanged (Fig. 4c). A similar pattern was observed in SW620 cells, where TAF1 deletion stabilized GPX4 protein expression (Figs. S4a and S4b), suggesting that TAF1 may regulate the degradation rather than the transcription of GPX4 protein. Confocal microscopy further confirmed that TAF1 promoted the degradation of nGPX4 (Figs. 4d and S4c). Consistently, the cycloheximide (CHX) chase assays demonstrated that TAF1 accelerated GPX4 degradation (Figs. 4e and S4d) and reduced its protein half-life (Figs. S4e and S4f).

Since GPX4 degradation can occur through either the ubiquitin-proteasome pathway (Sun XF et al., 2023; Wang et al., 2023) or autophagy (Wu et al., 2019; Xue et al., 2023), we next sought to determine which mechanism was involved in TAF1-mediated GPX4 turnover. Co-treatment of SKOV3 and SW620 cells with RSL3 and either the proteasome inhibitor MG132 or the autophagy inhibitor CQ revealed that only MG132 restored the GPX4 protein levels (Figs. 4f and S4g).

Collectively, these findings indicate that TAF1 promotes the degradation of nGPX4 via the ubiquitin-proteasome system in *TP53*-mutant cells, thereby modulating ferroptosis independently of transcriptional regulation.

2.5 TAF1-mediated K11-linked ubiquitination of nGPX4

In order to determine whether TAF1 interacts with and promotes nGPX4 ubiquitination, we co-transfected FLAG-tagged TAF1 and hemagglutinin (HA)-tagged nGPX4 into the human embryonic kidney 293T (HEK293T) cells. Immunoprecipitation assays confirmed that HA-nGPX4 was pulled down by FLAG-TAF1 (Fig. 5a). Conversely, FLAG-nGPX4 co-precipitated

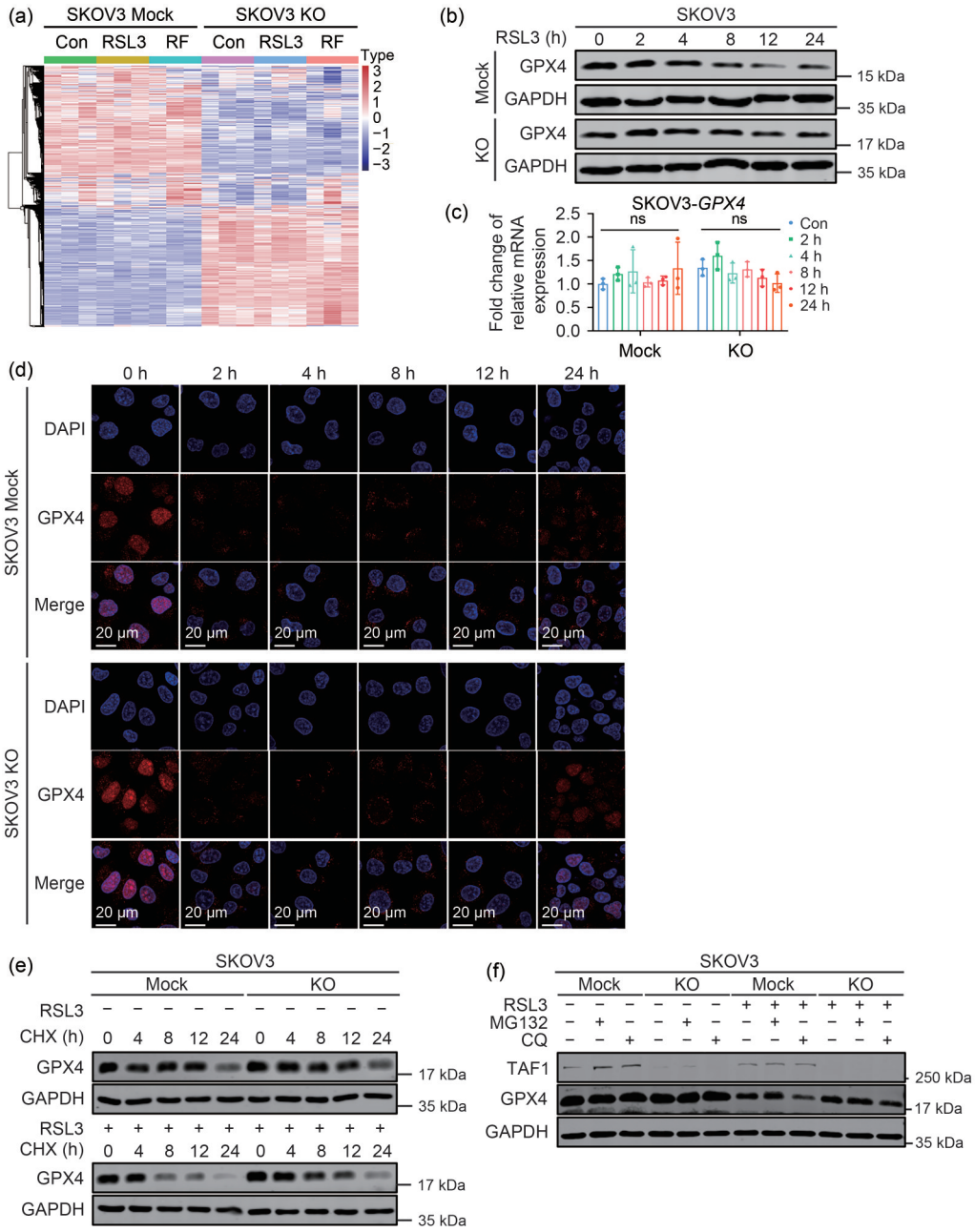

Fig. 4 TATA box-binding protein-associated factor 1 (TAF1)-mediated regulation of ferroptosis in tumor protein p53 (*TP53*)-mutant cells via ubiquitin-proteasome-mediated degradation of nuclear glutathione peroxidase 4 (nGPX4). (a) Heatmap showing differentially expressed genes (DEGs) in SKOV3 TAF1-Mock and TAF1-knockout (KO) cells treated with the indicated agents. Con: control; RSL3: (1S,3R)-RAS-selective lethal 3; RF: RSL3+ferrostatin-1. (b) Western blotting (WB) analysis of GPX4 protein levels in SKOV3 TAF1-Mock and TAF1-KO cells treated with 100 nmol/L RSL3 for the indicated times. (c) Fold changes in the relative *GPX4* messenger RNA (mRNA) levels in SKOV3 TAF1-Mock and TAF1-KO cells treated with 100 nmol/L RSL3 for the indicated times. All experiments were performed in triplicate. The data are presented as mean±standard deviation (SD). ns (not significant), $P>0.05$; one-way analysis of variance (ANOVA). (d) Immunofluorescence staining of GPX4 in SKOV3 TAF1-Mock and TAF1-KO cells treated with 100 nmol/L RSL3 for the indicated times. (e) WB analysis of GPX4 protein stability in SKOV3 TAF1-Mock and TAF1-KO cells treated with 100 nmol/L RSL3 for 4 h, followed by incubation with 50 μg/mL cycloheximide (CHX) for the indicated durations. (f) WB analysis of GPX4 protein levels in SKOV3 TAF1-Mock and TAF1-KO cells treated with 100 nmol/L RSL3 for 24 h, followed by co-treatment with 10 μmol/L MG132 or 25 μmol/L chloroquine (CQ) for 4 h. GAPDH: glyceraldehyde-3-phosphate dehydrogenase; DAPI: 4',6-diamidino-2-phenylindole.

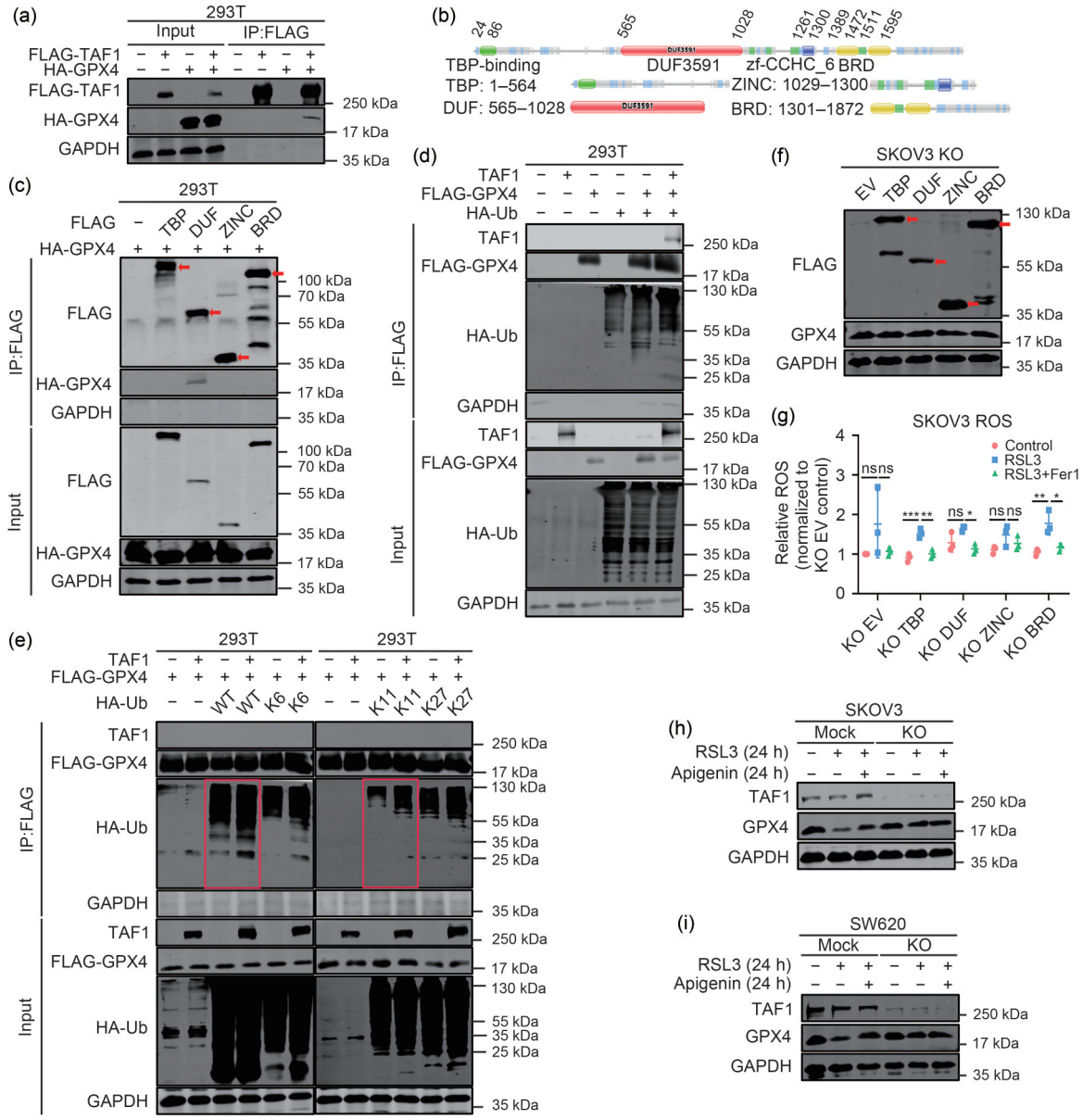

Fig. 5 TATA box-binding protein-associated factor 1 (TAF1)-mediated lysine 11 (K11)-linked ubiquitination of nuclear glutathione peroxidase 4 (nGPX4). (a) Western blotting (WB) analysis showing the co-immunoprecipitation (IP) of exogenous FLAG-tagged TAF1 and hemagglutinin (HA)-tagged nGPX4 in HEK293T cells. (b) Schematic representation of truncated TAF1 constructs. (c) WB analysis showing the co-IP of exogenous FLAG-tagged TAF1 truncations (indicated by red arrows), designed based on the domain architecture shown in (b), with HA-tagged nGPX4 in HEK293T cells. (d) Ubiquitination assay of FLAG-tagged nGPX4 in the presence of green fluorescent protein (GFP)-tagged TAF1. (e) HEK293T cells were co-transfected with GFP-TAF1 and FLAG-nGPX4 together with either wild-type (WT) ubiquitin (Ub) or the indicated Ub mutants. After treatment with MG132 (10 μmol/L) for 4 h, the cells were harvested for IP and WB analysis. The red box highlights the protein with the most pronounced change. (f) WB analysis of exogenous FLAG-tagged truncated TAF1 proteins (indicated by red arrows) expressed in SKOV3 TAF1-knockout (KO) cells. (g) Intracellular reactive oxygen species (ROS) levels in SKOV3 TAF1-KO cells transfected with different FLAG-tagged TAF1 truncations and treated with the indicated agents for 24 h. All experiments were performed in triplicate. The data are presented as mean±standard deviation (SD). $^{*}P<0.05$; $^{**}P<0.01$; $^{***}P<0.001$; ns (not significant), $P>0.05$; one-way analysis of variance (ANOVA). (h) WB analysis of GPX4 in SKOV3 TAF1-Mock and TAF1-KO cells treated with 100 nmol/L (1S,3R)-RAS-selective lethal 3 (RSL3) and 10 μmol/L apigenin for 24 h. (i) WB analysis of GPX4 in SW620 TAF1-Mock and TAF1-KO cells treated with 2.5 μmol/L RSL3 and 20 μmol/L apigenin for 24 h. TBP: TATA box-binding protein; DUF: domain of unknown function; ZINC: zinc finger domain; BRD: bromodomain; GAPDH: glyceraldehyde-3-phosphate dehydrogenase; EV: empty vector; Fer1: ferrostatin-1.

with green fluorescent protein (GFP)-TAF1 (Fig. S5a), further validating their interaction. Based on Pfam annotations (Mistry et al., 2021), we constructed four FLAG-tagged truncated TAF1 variants, each containing one of the following domains: the N-terminal kinase domain (FLAG-TBP (TBP: TATA box-binding protein)), the HAT domain (FLAG-DUF (DUF: domain of unknown function)), the E1/E2 domain (FLAG-ZINC (ZINC: zinc finger domain)), or the C-terminal kinase domain (FLAG-BRD (BRD: bromodomain)) (Fig. 5b). Immunoprecipitation assays showed that FLAG-DUF, but not FLAG-ZINC, interacted with HA-nGPX4 (Figs. 5c and S5b).

Notably, the overexpression of full-length TAF1 markedly increased the ubiquitination of nGPX4 (Fig. 5d). As polyubiquitin chains can be linked through seven distinct lysine residues (K6, K11, K27, K29, K33, K48, and K63) of ubiquitin (Mevissen and Komander, 2017), we generated seven HA-tagged ubiquitin mutants, each containing only a single lysine residue. Co-transfection of these mutants with FLAG-nGPX4 and GFP-TAF1 in HEK293T cells revealed that TAF1 overexpression specifically enhanced the K11-linked polyubiquitination of nGPX4 (Figs. 5e and S5c). Collectively, these findings demonstrate that TAF1 mediates the K11-linked ubiquitination of nGPX4, thereby facilitating its degradation.

In order to assess whether the DUF domain of TAF1 contributes to ferroptosis regulation, we overexpressed the four FLAG-tagged truncated TAF1 variants in SKOV3 TAF1-KO cells (Fig. 5f). Following treatment with RSL3 or RSL3 combined with ferrostatin-1, the intracellular ROS levels were measured. Remarkably, only the overexpression of FLAG-TBP and FLAG-BRD, which harbor the N- and C-terminal kinase domains, respectively, increased the sensitivity of SKOV3 TAF1-KO cells to RSL3-induced ferroptosis (Fig. 5g). These results suggest that the kinase domains of TAF1 play a crucial role in ferroptosis regulation.

In order to further explore the role of TAF1 kinase activity, TAF1-Mock and TAF1-KO cells of SKOV3 and SW620 were treated with RSL3 in the presence or absence of apigenin, a known inhibitor of TAF1 kinase activity (Li et al., 2004). Western blot analysis showed that apigenin effectively prevented GPX4 degradation induced by RSL3 treatment (Figs. 5h and 5i). Together, these findings demonstrate that TAF1 promotes GPX4 degradation via its kinase domain, thereby regulating ferroptosis in *TP53*-mutant cells.

2.6 TAF1-mediated enhancement of ferroptosis in *TP53*-mutant xenografts

Given that TAF1 promotes ferroptosis in *TP53*-mutant cells in vitro, we next investigated its role in vivo. For this purpose, subcutaneous xenograft tumors were established in nude mice using SW620 TAF1-Mock and TAF1-KO cells (Fig. 6a). Treatment with RSL3 markedly suppressed tumor growth in the TAF1-Mock group, whereas no significant inhibition was observed in the TAF1-KO group (Figs. 6b and 6c). Although RSL3 treatment tended to reduce tumor weight in the TAF1-Mock group, no such trend was evident in the TAF1-KO group (Fig. 6d). While these differences were not statistically significant, the data suggest that TAF1 KO confers resistance to RSL3-induced tumor suppression. Furthermore, immunohistochemical analysis revealed reduced GPX4 expression and increased 4-hydroxynonenal (4-HNE) accumulation in TAF1-Mock tumors following RSL3 treatment, whereas GPX4 and 4-HNE levels remained largely unchanged in TAF1-KO tumors (Fig. 6e). Collectively, these findings indicate that TAF1 enhances ferroptosis in vivo in *TP53*-mutant xenograft models.

3 Discussion

Ferroptosis, a distinct form of regulated cell death characterized by plasma membrane rupture due to the aberrant accumulation of iron-dependent phospholipid hydroperoxides (Yan et al., 2021), has been implicated in tumor suppression and increased sensitivity to chemotherapy (Roh et al., 2016, 2017; Sun et al., 2016; Sato et al., 2018). Despite its clinical significance, the molecular mechanisms governing ferroptosis remain incompletely understood. In this study, we identified TAF1 as a critical regulator of ferroptosis that exerts dual functions depending on the *TP53* status of cells. In *TP53*-mutant cells, TAF1 promotes the K11-linked ubiquitination and subsequent degradation of nGPX4, thereby facilitating ferroptosis. Conversely, in *TP53*-WT cells, TAF1 enhances MDM2-mediated TP53 degradation, resulting in *SLC7A11* upregulation and resistance to ferroptosis (Fig. 7).

TAF1, the largest subunit of the TFIID complex, participates in diverse cellular processes including phosphorylation, histone acetylation, ubiquitin activation, and ubiquitin conjugation. Beyond its established role in

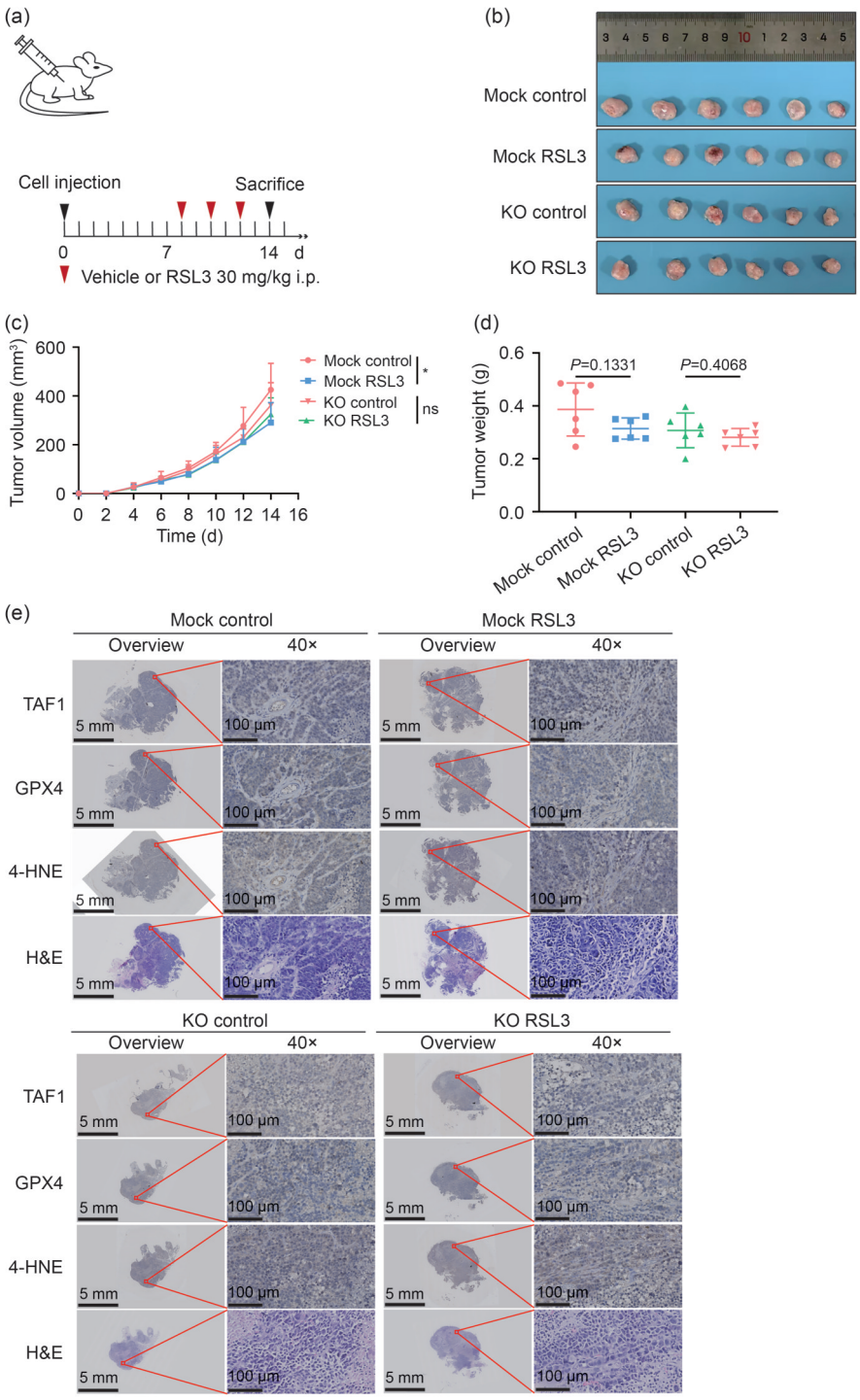

Fig. 6 TATA box-binding protein-associated factor 1 (TAF1)-mediated enhancement of ferroptosis in tumor protein p53 (*TP53*)-mutant xenografts. (a) Schematic illustration of the experimental design showing the establishment of subcutaneous xenograft tumors in nude mice and the treatment regimen. i.p.: intraperitoneal. (b) Representative images of tumors derived from SW620 TAF1-Mock and TAF1-knockout (KO) cells in mice treated with or without (1S,3R)-RAS-selective lethal 3 (RSL3) (n=6). (c) Tumor growth curves showing the xenograft volumes measured over time (n=6). $^{*}P$<0.05; ns (not significant), P>0.05. (d) Final tumor weights measured at the experimental endpoint (n=6). The data are presented as mean±standard deviation (SD). (e) Representative immunohistochemical staining of TAF1, glutathione peroxidase 4 (GPX4), and 4-hydroxynonenal (4-HNE), as well as hematoxylin and eosin (H&E) staining of TAF1-Mock and TAF1-KO xenograft tumors.

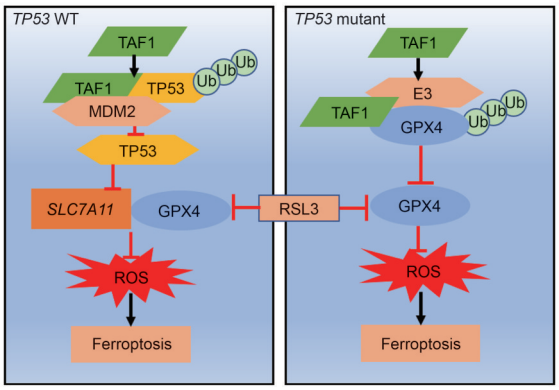

Fig. 7 Schematic illustration of TATA box-binding protein-associated factor 1 (TAF1)-mediated ferroptosis regulation. TAF1 promotes ferroptosis in tumor protei p53 (*TP53*)-mutant cells by facilitating the lysine 11 (K11)-linked ubiquitination and subsequent degradation of nuclear glutathione peroxidase 4 (nGPX4). In *TP53*-wild-type (WT) cells, TAF1 enhances the murine double minute 2 (MDM2)-mediated degradation of TP53, leading to the upregulation of solute carrier family 7 member 11 (*SLC7A11*) expression and conferring resistance to ferroptosis. ROS: reactive oxygen species; RSL3: (1S,3R)-RAS-selective lethal 3; Ub: ubiquitin; E3: ligase.

neurodegenerative diseases, TAF1 has been implicated in tumorigenesis: it promotes colon cancer cell proliferation by facilitating G1-phase progression through TP53 phosphorylation (Li et al., 2004) and contributes to leukemogenesis by acetylating the fusion transcription factor acute myeloid leukemia 1 protein (AML1)-eight twenty one protein (ETO) (Xu et al., 2019). TAF1 enhances epithelial–mesenchymal transition (EMT) in non-small-cell lung cancer (NSCLC) (Zhang et al., 2022) and increases paclitaxel resistance in esophageal cancer (Zhang et al., 2023). Moreover, the inhibition of TAF1 induces apoptosis (Zhou et al., 2021) and autophagy (Liu and Gu, 2022). However, the relationship between TAF1 and ferroptosis has remained unexplored. Our study reveals that TAF1 exhibits context-dependent functions in ferroptosis based on *TP53* status, highlighting its potential as a therapeutic target for ferroptosis-related interventions. Notably, several TAF1 inhibitors, such as BAY-299 (Zhou et al., 2021; Dibra et al., 2024), N2817 (Su et al., 2023), and BI-2536 (Puglisi et al., 2012), have demonstrated potent anticancer activity, while whether these inhibitors also modu-late ferroptosis warrants further investigation.

The TP53 protein is known as a key regulator of ferroptosis, orchestrating both canonical and noncanonical pathways (Liu and Gu, 2022); however, its role in ferroptotic regulation is complex, especially in metabolic contexts. WT TP53 represses *SLC7A11* expression, thereby promoting ferroptosis. An acetylation-defective mutant, $TP53^{3KR}$, retains this ability (Jiang et al., 2015), whereas other hotspot mutations impair ferroptotic sensitivity. For example, $TP53^{R172H}$ and $TP53^{R245W}$ suppress ferroptosis via the NRF2-dependent regulation of microsomal glutathione *S*-transferase 3 (MGST3) and peroxiredoxin 6 (PRDX6) (Dibra et al., 2024), while $TP53^{R175H}$ enhances tumor growth by binding to and inhibiting BTB and CNC homology 1 (BACH1)-mediated *SLC7A11* downregulation (Su et al., 2023). Our findings further indicate that the functional outcome of TAF1 depends on *TP53* status. In *TP53*-WT cells, TAF1 facilitates the MDM2-mediated degradation of phosphorylated TP53, leading to the upregulation of *SLC7A11* and resistance to ferroptosis—consistent with previous observations (Jiang et al., 2015). In contrast, in *TP53*-null (SKOV3) and *TP53*-mutant (SW620, harboring $TP53^{R273H}$ and $TP53^{P309S}$ mutations) cells, TAF1 phosphorylates and promotes the degradation of nuclear GPX4, thereby triggering ferroptosis. Given that TAF1 phosphorylates both TP53 and GPX4, and that TP53 can directly interact with GPX4 (Qian et al., 2023), we propose that TP53 and nGPX4 may compete for TAF1 binding. The precise molecular mechanisms underlying this competition, however, require further elucidation.

GPX4 exists in three major isoforms localized in the cytosol (cGPX4), mitochondria (mGPX4), and nucleus (nGPX4), respectively (Xie et al., 2023). While cGPX4 and mGPX4 have been studied extensively, the physiological role of nGPX4 remains poorly understood. Initially identified in murine male germ cells, nGPX4 associates with the sperm nuclear matrix and facilitates chromatin decondensation during fertilization (Puglisi et al., 2012). More recently, nGPX4—also referred to as inducible GPX4 (iGPX4)—was reported to promote ferroptosis in metabolic-associated fatty liver disease (MAFLD) by driving cGPX4 oligomerization into enzymatically inactive complexes (Tong et al., 2022). In contrast, our study uncovers a previously unrecognized protective role of nGPX4, namely that it acts as a nuclear antioxidant defense against phospholipid hydroperoxide-induced ferroptosis. This finding challenges the prevailing view of nGPX4 as a pro-ferroptotic factor and suggests that nuclear GPX4 may exert context-dependent regulatory functions in ferroptosis.

Previous research has identified several mechanisms governing GPX4 degradation. Members of the

tripartite motif (TRIM) protein family, including TRIM25 (Li et al., 2023) and TRIM26 (Wang et al., 2023), catalyze GPX4 ubiquitination and degradation. Additionally, chaperone-mediated autophagy contributes to GPX4 turnover (Wu et al., 2019). However, these studies focus primarily on cGPX4 and mGPX4, leaving the regulatory mechanisms of nGPX4 largely unexplored. Herein, we demonstrated that TAF1 directly mediates nGPX4 degradation in *TP53*-mutant cells by promoting its K11-linked polyubiquitination and subsequent proteasomal degradation, representing a novel pathway by which TAF1 regulates ferroptosis in the context of *TP53* mutation.

Despite these promising findings, several key questions remain. First, we observed that TAF1-mediated nGPX4 degradation occurred only upon RSL3 treatment. RSL3 has been regarded as a selective GPX4 inhibitor that covalently binds to the enzyme's active site, thereby suppressing its catalytic activity (Yang et al., 2014, 2016). However, a recent report suggested that RSL3 does not directly inhibit GPX4 activity but rather alters its electrophoretic migration in gels (Cheff et al., 2023). This observation implies that RSL3 may chemically modify GPX4, and we speculate that such modification enhances the interaction between TAF1 and GPX4. Nevertheless, the exact mechanism remains unclear, and further biochemical and structural investigations are required to elucidate the underlying processes. Moreover, although TAF1 promotes nGPX4 ubiquitination and degradation, the specific ubiquitin-activating enzyme (E1), -conjugating enzyme (E2), and ligase (E3) involved have not yet been identified. Given that TAF1 contains intrinsic kinase and ubiquitin-related domains, it is plausible that TAF1 itself may function as an E1 or E2 enzyme within this pathway. Therefore, identifying the E3 ligase responsible for nGPX4 ubiquitination will be an important direction of future research.

4 Conclusions

This study provides critical insights into the molecular mechanisms regulating ferroptosis and establishes a foundation for precision medicine approaches. In *TP53*-WT tumors, low TAF1 expression may serve as a predictive biomarker for the efficacy of ferroptosis-based therapies. Conversely, in *TP53*-mutant tumors with high TAF1 expression, patients may benefit more from treatment with ferroptosis inducers. Collectively, our study highlights the potential of targeting TAF1 to develop genotype-specific ferroptosis-based therapeutic strategies, paving the way for more effective and personalized cancer treatment options.

Materials and methods

Detailed methods are provided in the electronic supplementary materials of this paper.

Data availability statement

Total RNA expression profiling data from 12 OV patients and 57 healthy donors were obtained from the GSE66957 dataset available in the Gene Expression Omnibus (GEO) database (https://www.ncbi.nlm.nih.gov/geo/query/acc.cgi?acc=GSE66957). In addition, the TCGA OV and COAD datasets were retrieved from the UCSC Xena platform (https://xenabrowser.net). The RNA-seq data of SKOV3 TAF1-Mock and TAF1-KO cell lines following RSL3 or RSL3+ferrostatin-1 treatment have been deposited into the Sequence Read Archive (SRA) database and can be accessed at https://www.ncbi.nlm.nih.gov/bioproject/PRJNA1231572. All other research data can be obtained from the authors upon reasonable request.

Acknowledgments

This work was supported by the National Natural Science Foundation of China (Nos. 82473008, 82173223, and 82303644), the Chinese Academy of Medical Sciences (CAMS) Innovation Fund for Medical Sciences (No. 2019-I2M-5-044), and the Zhejiang Medical and Health Science and Technology Project (No. 2025KY439), China.

We thank Qiong HUANG from the Core Facilities, Zhejiang University School of Medicine for her technical support. We thank Shanghai Tengyun Biotechnology Co., Ltd. for developing Hiplot^{Pro} platform (https://hiplot.com.cn) and providing technical assistance and valuable tools for data analysis and visualization.

Author contributions

Kehong YE, Chaoyi CHEN, and Honghe ZHANG proposed the scientific question. Kehong YE, Chaoyi CHEN, and Liang SUN designed the experiments and conducted the research. Kehong YE, Xuan LAI, Yinjun HE, and Ming ZHU established the animal models. Kehong YE and Chaoyi CHEN performed the data analysis. Kehong YE drafted the manuscript, and Liang SUN and Xuan LAI assisted in manuscript revision. Honghe ZHANG, Chaoyi CHEN, and Meifu GAN provided funding support for the project. Honghe ZHANG and Weiqin JIANG conceived the overall study and coordinated the research team. All authors have read and approved the final manuscript, and therefore, have full access to all the data in the study and take responsibility for the integrity and security of the data.

Compliance with ethics guidelines

Honghe ZHANG is a Young Scientist Committee Member for *Journal of Zhejiang University-SCIENCE B* and was not involved in the editorial review or the decision to publish this article. Kehong YE, Meifu GAN, Liang SUN, Chaoyi CHEN, Xuan LAI, Yinjun HE, Ming ZHU, Weiqin JIANG, and Honghe ZHANG declare that they have no conflicts of interest.

All institutional and national guidelines for the care and use of laboratory animals were followed. All animal experiments were conducted in accordance with protocols approved by the Institutional Animal Care and Use Committee of Zhejiang University (Ethics Committee No. ZJU20240161).

Declaration on the use of generative AI tools

During the preparation of this work, the authors used DeepSeek and ChatGPT in order to improve language and readability. After using these tools, the authors reviewed and edited the content as needed and take full responsibility for the content of the publication.

References

Akoglu H, 2018. User's guide to correlation coefficients. *Turk J Emerg Med*, 18(3):91-93. https://doi.org/10.1016/j.tjem.2018.08.001

Aneichyk T, Hendriks WT, Yadav R, et al., 2018. Dissecting the causal mechanism of X-linked dystonia-parkinsonism by integrating genome and transcriptome assembly. *Cell*, 172(5):897-909.e21. https://doi.org/10.1016/j.cell.2018.02.011

Bersuker K, Hendricks JM, Li ZP, et al., 2019. The CoQ oxidoreductase FSP1 acts parallel to GPX4 to inhibit ferroptosis. *Nature*, 575(7784):688-692. https://doi.org/10.1038/s41586-019-1705-2

Cheff DM, Huang CY, Scholzen KC, et al., 2023. The ferroptosis inducing compounds RSL3 and ML162 are not direct inhibitors of GPX4 but of TXNRD1. *Redox Biol*, 62:102703. https://doi.org/10.1016/j.redox.2023.102703

Chen X, Kang R, Kroemer G, et al., 2021. Broadening horizons: the role of ferroptosis in cancer. *Nat Rev Clin Oncol*, 18(5):280-296. https://doi.org/10.1038/s41571-020-00462-0

Cheng HY, Capponi S, Wakeling E, et al., 2020. Missense variants in *TAF1* and developmental phenotypes: challenges of determining pathogenicity. *Hum Mutat*, 41(2):449-464. https://doi.org/10.1002/humu.23936

Deng F, Zhao BC, Yang X, et al., 2021. The gut microbiota metabolite capsiate promotes Gpx4 expression by activating *TRPV1* to inhibit intestinal ischemia reperfusion-induced ferroptosis. *Gut Microbes*, 13(1):1902719. https://doi.org/10.1080/19490976.2021.1902719

Dibra D, Xiong SB, Moyer SM, et al., 2024. Mutant p53 protects triple-negative breast adenocarcinomas from ferroptosis in vivo. *Sci Adv*, 10(7):eadk1835. https://doi.org/10.1126/sciadv.adk1835

Dikstein R, Ruppert S, Tjian R, 1996. $TAF_{II}250$ is a bipartite protein kinase that phosphorylates the basal transcription factor RAP74. *Cell*, 84(5):781-790. https://doi.org/10.1016/S0092-8674(00)81055-7

Dixon SJ, Lemberg KM, Lamprecht MR, et al., 2012. Ferroptosis: an iron-dependent form of nonapoptotic cell death. *Cell*, 149(5):1060-1072. https://doi.org/10.1016/j.cell.2012.03.042

Dixon SJ, Patel DN, Welsch M, et al., 2014. Pharmacological inhibition of cystine–glutamate exchange induces endoplasmic reticulum stress and ferroptosis. *eLife*, 3:e02523. https://doi.org/10.7554/eLife.02523

Doll S, Freitas FP, Shah R, et al., 2019. FSP1 is a glutathione-independent ferroptosis suppressor. *Nature*, 575(7784):693-698. https://doi.org/10.1038/s41586-019-1707-0

Feng ZW, Yang CF, Xiao HF, et al., 2024. YTHDC1 regulates the migration, invasion, proliferation, and apoptosis of rheumatoid fibroblast-like synoviocytes. *Front Immunol*, 15:1440398. https://doi.org/10.3389/fimmu.2024.1440398

Goldman MJ, Craft B, Hastie M, et al., 2020. Visualizing and interpreting cancer genomics data via the Xena platform. *Nat Biotechnol*, 38(6):675-678. https://doi.org/10.1038/s41587-020-0546-8

Guo YY, Liang NN, Zhang XY, et al., 2024. Mitochondrial GPX4 acetylation is involved in cadmium-induced renal cell ferroptosis. *Redox Biol*, 73:103179. https://doi.org/10.1016/j.redox.2024.103179

Hou W, Xie YC, Song XX, et al., 2016. Autophagy promotes ferroptosis by degradation of ferritin. *Autophagy*, 12(8):1425-1428. https://doi.org/10.1080/15548627.2016.1187366

Janakiraman U, Dhanalakshmi C, Yu J, et al., 2020. The investigation of the T-type calcium channel enhancer SAK3 in an animal model of TAF1 intellectual disability syndrome. *Neurobiol Dis*, 143:105006. https://doi.org/10.1016/j.nbd.2020.105006

Jiang L, Kon N, Li TY, et al., 2015. Ferroptosis as a p53-mediated activity during tumour suppression. *Nature*, 520(7545):57-62. https://doi.org/10.1038/nature14344

Kang YJ, Pan LJ, Liu YY, et al., 2025. GEPIA3: enhanced drug sensitivity and interaction network analysis for cancer research. *Nucleic Acids Res*, 53(W1):W283-W290. https://doi.org/10.1093/nar/gkaf423

Li HH, Li AG, Sheppard HM, et al., 2004. Phosphorylation on Thr-55 by TAF1 mediates degradation of p53: a role for TAF1 in cell G1 progression. *Mol Cell*, 13(6):867-878. https://doi.org/10.1016/S1097-2765(04)00123-6

Li JB, Liu J, Zhou Z, et al., 2023. Tumor-specific GPX4 degradation enhances ferroptosis-initiated antitumor immune response in mouse models of pancreatic cancer. *Sci Transl Med*, 15(720):eadg3049. https://doi.org/10.1126/scitranslmed.adg3049

Lin WJ, Li HH, Chang J, et al., 2025. ZC3H13 may participate in the ferroptosis process of sepsis-induced cardiomyopathy by regulating the expression of Pnn and Rbm25.

Gene, 933:148944.
https://doi.org/10.1016/j.gene.2024.148944

Liu YQ, Gu W, 2022. p53 in ferroptosis regulation: the new weapon for the old guardian. *Cell Death Differ*, 29(5): 895-910.
https://doi.org/10.1038/s41418-022-00943-y

Mao C, Liu XG, Zhang YL, et al., 2021. DHODH-mediated ferroptosis defence is a targetable vulnerability in cancer. *Nature*, 593(7860):586-590.
https://doi.org/10.1038/s41586-021-03539-7

Mevissen TET, Komander D, 2017. Mechanisms of deubiquitinase specificity and regulation. *Annu Rev Biochem*, 86: 159-192.
https://doi.org/10.1146/annurev-biochem-061516-044916

Mistry J, Chuguransky S, Williams L, et al., 2021. Pfam: the protein families database in 2021. *Nucleic Acids Res*, 49(D1): D412-D419.
https://doi.org/10.1093/nar/gkaa913

Mizzen CA, Yang XJ, Kokubo T, et al., 1996. The $TAF_{II}250$ subunit of TFIID has histone acetyltransferase activity. *Cell*, 87(7):1261-1270.
https://doi.org/10.1016/S0092-8674(00)81821-8

Newton K, Strasser A, Kayagaki N, et al., 2024. Cell death. *Cell*, 187(2):235-256.
https://doi.org/10.1016/j.cell.2023.11.044

Oh HR, An CH, Yoo NJ, et al., 2017. Frameshift mutations in the mononucleotide repeats of *TAF1* and *TAF1L* genes in gastric and colorectal cancers with regional heterogeneity. *Pathol Oncol Res*, 23(1):125-130.
https://doi.org/10.1007/s12253-016-0107-0

Pham AD, Sauer F, 2000. Ubiquitin-activating/conjugating activity of $TAF_{II}250$, a mediator of activation of gene expression in *Drosophila*. *Science*, 289(5488):2357-2360.
https://doi.org/10.1126/science.289.5488.2357

Puglisi R, Maccari I, Pipolo S, et al., 2012. The nuclear form of glutathione peroxidase 4 is associated with sperm nuclear matrix and is required for proper paternal chromatin decondensation at fertilization. *J Cell Physiol*, 227(4): 1420-1427.
https://doi.org/10.1002/jcp.22857

Qian B, Che L, Du ZB, et al., 2023. Protein phosphatase 2A-B55β mediated mitochondrial p-GPX4 dephosphorylation promoted sorafenib-induced ferroptosis in hepatocellular carcinoma via regulating p53 retrograde signaling. *Theranostics*, 13(12):4288-4302.
https://doi.org/10.7150/thno.82132

Ribeiro JR, Lovasco LA, Vanderhyden BC, et al., 2014. Targeting TBP-associated factors in ovarian cancer. *Front Oncol*, 4:45.
https://doi.org/10.3389/fonc.2014.00045

Roh JL, Kim EH, Jang HJ, et al., 2016. Induction of ferroptotic cell death for overcoming cisplatin resistance of head and neck cancer. *Cancer Lett*, 381(1):96-103.
https://doi.org/10.1016/j.canlet.2016.07.035

Roh JL, Kim EH, Jang H, et al., 2017. Nrf2 inhibition reverses the resistance of cisplatin-resistant head and neck cancer cells to artesunate-induced ferroptosis. *Redox Biol*, 11:254-262.
https://doi.org/10.1016/j.redox.2016.12.010

Sato M, Kusumi R, Hamashima S, et al., 2018. The ferroptosis inducer erastin irreversibly inhibits system x_c^- and synergizes with cisplatin to increase cisplatin's cytotoxicity in cancer cells. *Sci Rep*, 8:968.
https://doi.org/10.1038/s41598-018-19213-4

Schober P, Boer C, Schwarte LA, 2018. Correlation coefficients: appropriate use and interpretation. *Anesth Analg*, 126(5): 1763-1768.
https://doi.org/10.1213/ANE.0000000000002864

Spies J, Waizenegger A, Barton O, et al., 2016. Nek1 regulates Rad54 to orchestrate homologous recombination and replication fork stability. *Mol Cell*, 62(6):903-917.
https://doi.org/10.1016/j.molcel.2016.04.032

Su ZY, Kon N, Yi JJ, et al., 2023. Specific regulation of BACH1 by the hotspot mutant $p53^{R175H}$ reveals a distinct gain-of-function mechanism. *Nat Cancer*, 4(4):564-581.
https://doi.org/10.1038/s43018-023-00532-z

Sun BH, Wang XY, Ye ZQ, et al., 2023. Designing single-atom active sites on sp^2-carbon linked covalent organic frameworks to induce bacterial ferroptosis-like for robust antiinfection therapy. *Adv Sci*, 10(13):2207507.
https://doi.org/10.1002/advs.202207507

Sun XF, Niu XH, Chen RC, et al., 2016. Metallothionein-1G facilitates sorafenib resistance through inhibition of ferroptosis. *Hepatology*, 64(2):488-500.
https://doi.org/10.1002/hep.28574

Sun XF, Zhang Q, Lin XH, et al., 2023. Imatinib induces ferroptosis in gastrointestinal stromal tumors by promoting STUB1-mediated GPX4 ubiquitination. *Cell Death Dis*, 14:839.
https://doi.org/10.1038/s41419-023-06300-2

Tavassoli P, Wafa LA, Cheng H, et al., 2010. TAF1 differentially enhances androgen receptor transcriptional activity via its N-terminal kinase and ubiquitin-activating and -conjugating domains. *Mol Endocrinol*, 24(4):696-708.
https://doi.org/10.1210/me.2009-0229

Tong J, Li DJ, Meng HB, et al., 2022. Targeting a novel inducible GPX4 alternative isoform to alleviate ferroptosis and treat metabolic-associated fatty liver disease. *Acta Pharm Sin B*, 12(9):3650-3666.
https://doi.org/10.1016/j.apsb.2022.02.003

Wang H, Curran EC, Hinds TR, et al., 2014. Crystal structure of a TAF1-TAF7 complex in human transcription factor IID reveals a promoter binding module. *Cell Res*, 24(12): 1433-1444.
https://doi.org/10.1038/cr.2014.148

Wang HB, Qi WW, Zou CY, et al., 2021. NEK1-mediated retromer trafficking promotes blood–brain barrier integrity by regulating glucose metabolism and RIPK1 activation. *Nat Commun*, 12:4826.
https://doi.org/10.1038/s41467-021-25157-7

Wang RP, Song SM, Harada K, et al., 2020. Multiplex profiling of peritoneal metastases from gastric adenocarcinoma identified novel targets and molecular subtypes that predict treatment response. *Gut*, 69(1):18-31.
https://doi.org/10.1136/gutjnl-2018-318070

Wang WL, Liu Y, Wang ZQ, et al., 2024. Exploring and validating the necroptotic gene regulation and related lncRNA

mechanisms in colon adenocarcinoma based on multi-dimensional data. *Sci Rep*, 14:22251. https://doi.org/10.1038/s41598-024-73168-3

Wang ZJ, Xia Y, Wang Y, et al., 2023. The E3 ligase TRIM26 suppresses ferroptosis through catalyzing K63-linked ubiquitination of GPX4 in glioma. *Cell Death Dis*, 14(10):695. https://doi.org/10.1038/s41419-023-06222-z

Wu ZM, Geng Y, Lu XJ, et al., 2019. Chaperone-mediated autophagy is involved in the execution of ferroptosis. *Proc Natl Acad Sci USA*, 116(8):2996-3005. https://doi.org/10.1073/pnas.1819728116

Xie XX, Chen CC, Wang C, et al., 2024. Targeting GPX4-mediated ferroptosis protection sensitizes *BRCA1*-deficient cancer cells to PARP inhibitors. *Redox Biol*, 76:103350. https://doi.org/10.1016/j.redox.2024.103350

Xie YC, Kang R, Klionsky DJ, et al., 2023. GPX4 in cell death, autophagy, and disease. *Autophagy*, 19(10):2621-2638. https://doi.org/10.1080/15548627.2023.2218764

Xu Y, Man N, Karl D, et al., 2019. TAF1 plays a critical role in AML1-ETO driven leukemogenesis. *Nat Commun*, 10:4925. https://doi.org/10.1038/s41467-019-12735-z

Xue Q, Yan D, Chen X, et al., 2023. Copper-dependent autophagic degradation of GPX4 drives ferroptosis. *Autophagy*, 19(7):1982-1996. https://doi.org/10.1080/15548627.2023.2165323

Yan B, Ai YW, Sun Q, et al., 2021. Membrane damage during ferroptosis is caused by oxidation of phospholipids catalyzed by the oxidoreductases POR and CYB5R1. *Mol Cell*, 81(2):355-369.e10. https://doi.org/10.1016/j.molcel.2020.11.024

Yang LX, Song TJ, Cheng Q, et al., 2019. Mutant p53 sequestration of the MDM2 acidic domain inhibits E3 ligase activity. *Mol Cell Biol*, 39(4):e00375-18. https://doi.org/10.1128/MCB.00375-18

Yang WS, SriRamaratnam R, Welsch ME, et al., 2014. Regulation of ferroptotic cancer cell death by GPX4. *Cell*, 156(1-2):317-331. https://doi.org/10.1016/j.cell.2013.12.010

Yang WS, Kim KJ, Gaschler MM, et al., 2016. Peroxidation of polyunsaturated fatty acids by lipoxygenases drives ferroptosis. *Proc Natl Acad Sci USA*, 113(34):E4966-E4975. https://doi.org/10.1073/pnas.1603244113

Zang X, He XY, Xiao CM, et al., 2024. Circular RNA-encoded oncogenic PIAS1 variant blocks immunogenic ferroptosis by modulating the balance between SUMOylation and phosphorylation of STAT1. *Mol Cancer*, 23:207. https://doi.org/10.1186/s12943-024-02124-6

Zhang J, Li R, Zhang BX, et al., 2022. TAF1 promotes NSCLC cell epithelial-mesenchymal transition by transcriptionally activating TGFβ1. *Biochem Biophys Res Commun*, 636(Pt 2):113-118. https://doi.org/10.1016/j.bbrc.2022.10.099

Zhang SY, Zhong JY, Guo DN, et al., 2023. MIAT shuttled by tumor-secreted exosomes promotes paclitaxel resistance in esophageal cancer cells by activating the TAF1/SREBF1 axis. *J Biochem Mol Toxicol*, 37(8):e23380. https://doi.org/10.1002/jbt.23380

Zhou LX, Yao Q, Ma L, et al., 2021. TAF1 inhibitor Bay-299 induces cell death in acute myeloid leukemia. *Transl Cancer Res*, 10(12):5307-5318. https://doi.org/10.21037/tcr-21-2295

Supplementary information

Materials and methods; Figs. S1–S5